Research Paper DOI: http://dx.doi.org/10.6108/KSPE.2015.19.6.042

# 나노 알루미늄 입자 첨가 추진제에 의한 탄소복합재 노즐의 기계적 삭마 감소 특성 예측

Prashant Tarey[a] · 김재호[a] · Valery I. Levitas[b] · 하동성[c] · 박재현[d] · 양희성[a,*]

# Prediction of the Mechanical Erosion Rate Decrement for Carbon-Composite Nozzle by using the Nano-Size Additive Aluminum Particle

Prashant Tarey[a] · Jaiho Kim[a] · Valeny I. Levitas[b] · Dongsung Ha[c] · Jae Hyun Park[d] · Heesung Yang[a,*]

[a]*Research Division, Seyeon Engineering and System, Korea*
[b]*Department of Aerospace Engineering, Iowa State University, USA*
[c]*The 4th R&D Institute, Agency for Defense Development, Korea*
[d]*Department of Aerospace and Software Engineering and Research Center for Aircraft Parts Technology, Gyeongsang National University, Korea*
[*]*Corresponding author. E-mail: hsyang@seyeon-ens.com*

## ABSTRACT

In this study, the influence of Al particle size, as an additive for solid propellant, on the mechanical erosion of the carbon-composite nozzle was evaluated. A new model which can predict the size and distribution of the agglomerated reaction product($Al(l)/Al_2O_3(l)$) was established, and the size of agglomerate were calculated according to the various initial size of Al in the solid propellant. With predicted results of the model, subsequently, the characteristics of mechanical erosion on the carbon-composite nozzle was estimated using a commercial CFD software, STAR CCM+. The result shows that the smaller the initial Al particles are, in the solid propellant, the lower is the mechanical erosion rate of the composite nozzle wall, especially for the nano-size Al particle.

## 초 록

고체추진제에 첨가되는 알루미늄 입자의 크기에 따른 탄소 복합재 노즐의 기계적 삭마특성 변화를 예측하는 연구를 수행하였다. 추진제에 첨가되는 알루미늄 입자의 초기 크기에 따라 연소생성물 응집체($Al(l)/Al_2O_3(l)$)의 크기와 분포를 예측할 수 있는 모델을 개발하여 사용하였으며, 모델 예측 결과로 얻어지는 응집체의 크기를 초기조건으로 하여 상용 수치해석 프로그램(STAR CCM+)을 이용한 복합재 노즐에서의 기계적 삭마특성 해석을 수행하였다. 본 연구를 통해 초기 알루미늄 첨가제의 크기가 작을수록 응집체의 크기가 작아지고, 기계적 삭마가 감소하는 특성을 확인하였으며, 특히 나노입자를 사용할 때 기계적 삭마가 확연히 개선됨을 확인하였다.

Key Words: Solid Rocket Motor(고체로켓모터), Mechanical Erosion(기계적 삭마), Aluminum Particle(알루미늄입자), Agglomeration(응집체)

Received 23 September 2015 / Revised 2 November 2015 / Accepted 6 November 2015

pISSN 1226-6027 / eISSN 2288-4548

## 1. Introduction

Composite solid fuels are widely used in propulsion systems for rockets, missiles and launch vehicle. They have several advantages, like simple structure, high energy density, compactness and low cost. Specific impulse(Isp) can be used as a parameter to compare the performance of different propellants. Fuels with higher Isp will reduce the weight of the vehicle, increase the efficiency and reduce the overall cost of the mission. For these reasons, metal powder additives of aluminum and boron are used as fuel components depending on mission objectives. Ammonium perchlorate(AP) is one of the most widely used oxidizer because of its high performance, compatibility with other propellants and availability. Binder is a rubbery polymer matrix to hold all the fuel components in a compact form. It also acts as a fuel, which gets oxidized and produces combustion gases. HTPB is most commonly used because of its excellent physical properties.

During combustion of solid propellant, a mobile liquid layer is formed at the burning fuel surface, where aluminum particle melts and agglomerates to form bigger particle[1]. A part of aluminum agglomerates gets completely oxidized either at the fluidized bed or shortly after entering the gas phase. The remaining aluminum agglomerates get covered by an oxide layer. Formation of an oxide layer hinders its combustion. As the temperature of the particles increases, aluminum melts, expands and breaks the outer oxide shell. Subsequently, the liquid aluminum exposed to the gas oxidizers ignites with a characteristic flame. Some residual agglomerates exit the motor without any combustion. This unburnt aluminum does not contribute in enhancing the specific impulse and results only in two phase losses. The size of the agglomerates is determined by the quantity, diameter and ignition time of the aluminum particles[1]. Other influencing factors are thickness of the fluidized bed and operating chamber conditions.

The Al(l) agglomerates and $Al(l)/Al_2O_3(l)$ droplets reduce the combustion instabilities in the gas phase. However, they also result in mechanical erosion on the graphite or C-C composite nozzle wall[1]. Moreover, the Graphite and the C-C composite nozzle wall undergo significant erosion due to impingement of $Al(l)/Al_2O_3(l)$-droplets at the convergent part of the nozzle[2]. For these reasons, the agglomeration phenomena need indepth understanding. However, lack of experimental data and inherent unsteadiness of combustion phenomenon poses serious challenges in this field of research. Carrying out experimental research work is not only extremely complex but also very expensive. In spite of these difficulties, a significant effort has been made as follows: high speed photography to study agglomeration in metalized solid propellants by Crump et al.[3] and Gany et al.[4], a comprehensive review on metallized propellant combustion by Price[5], relationship between agglomeration phenomenon and slag formation by Boraas[6] and Salita[7], a detailed review by Beckstead[8], “Pocket model” by Cohen[9,10] and a stochastic method to determine the cluster volume by Gallier[11]. In particular, the agglomeration models can be divided into two broad categories. One is to predict the size of the aggregates by the geometric shape of the binder and aluminum particles of the solid propellant (pocket model)[9,10]. Another is a theory that the characteristic of aggregation is determined by the combustion and mechanism

of Al accumulation in the thin mobile layer of the propellant surface[1].

The present work attempts to develop a new model which combines the aforementioned two theoretical models, including not only prediction of the mean $Al(l)/Al_2O_3(l)$ droplet size but also prediction of distribution based on recent nano-size combustion model. With the result of the newly developed agglomeration model, the STAR CCM+ model based on the work by Thakre et al.[12] was used to predict the mechanical ablation. Erosion rate for different values of $Al(l)/Al_2O_3(l)$-droplet diameter is also calculated.

## 2. Agglomeration Model Formulation

### 2.1 Agglomeration Model

Solid propellant like AP/HTPB and AP/HTPB with small percentage of aluminum(~15%), pass through complex chemical and physical phenomena during combustion. A hot liquid bed is formed at the burning fuel surface. The aluminum particle agglomeration phenomenon takes place in this fluidized bed. The diameter of the aluminum agglomerates is determined by the number of Al-particles that can agglomerate in the fluidized bed before ignition. If the thickness of the fluidized bed '$l$' is larger than the initial diameter '$d$' of Al-particles, the diameter '$D_{ag}$' of the aggregate will be given by the following formula[1]:

$$D_{ag} = \sqrt[3]{\left[\frac{6lD_e^2}{\pi\beta} - d^3\right]N_{ag} + d^3} \quad (1)$$

Where, '$D_e$' is the characteristic length of the fluidized bed, '$\beta$' is the geometric volume ratio of the aluminum particles and '$N_{ag}$' is the number of particles forming the agglomerate. The thickness of the fluid bed '$l$' can be determined experimentally or theoretically. Here, a theoretical model for composite propellants was used[13], and the equation was re-calculated from the graph in Ref.[13].

$$l = 6.80907 + 74.48278\exp\left(-\frac{p-0.65822}{17.18901}\right) \quad (2)$$

Here, the thickness '$l$' is in $\mu m$ and '$p$' is in atm. The value of '$D_e$' is given by the following formula:

$$D_e = \sqrt{A_{e,t} + A_{e,b}} = \sqrt{D_{e,\max}^2 - \frac{\pi l}{2}(D_{AP} - l)} \quad (3)$$

'$D_{AP}$' is the diameter of AP particles. '$D_{e,\max}$' is the arithmetic mean of simple cubic, face centered cubic(FCC) and body centered cubic(BCC) arrangements, and is given by Yavor's method[1]:

$$D_{e,\max} = \frac{1 + \sqrt{2} + \frac{2}{\sqrt{3}}}{3} D_{AP} \quad (4)$$

'$N_{ag}$' the aggregation number, which is the ratio of '$t_{ig}$' and '$t_{ac}$'.

$$N_{ag} = \frac{t_{ig}}{t_{ac}} = \frac{t_{ig}\dot{r}\beta\phi}{l(1-\beta\phi)} \quad (5)$$

Here, '$t_{ig}$' is the ignition time of aluminum particles and '$t_{ac}$' is the time to accumulate the aluminum particle on the fluid bed, '$\dot{r}$' is the burning rate of the propellant and '$\phi$' is the volume occupied by aluminum in the propellant. For particle size greater than 10

$\mu m$, the alumina covering the aluminum melts approximately at 2300 $K$[14]. For nano sized particles, the melting temperature is below 2300 $K$. Here, the ignition temperature is calculated by the following formula[15]:

$$t_{ig} = \frac{\rho_{Al}(c\Delta T + L)}{hA_{ex}} \tag{6}$$

Here, '$\rho_{Al}$' is the density of aluminum, '$c$' is the heat capacity of aluminum, '$\triangle T$' is the difference between the ignition temperature and the initial temperature of aluminum particles, '$L$' is the latent heat of aluminum, '$h$' is the heat flux transferred to the propellant surface from the diffusion flame, '$A_{ex}$' is the area exposed to the propellant gas of the aluminum particles floating in the fluid bed. In this study, the value of heat flux '$h$' is the curve fitting function from the combustion model of the AP/HTPB/Al propellant. The value of '$h$' is approximated by the following function[13]:

$$h = 31.38\, p^{0.862} \tag{7}$$

'$A_{ex}$' is calculated by the force balance between the aluminum particles which are floating on the fluid bed by buoyancy, with the assumption that the fluid bed is in a liquid state[15]:

$$A_{ex} = \frac{3\pi\mu_l \dot{r} d^2}{4\sigma_l} \tag{8}$$

Where '$\mu_l$' is the viscosity of the fluid bed and '$\sigma_l$' is the surface tension.

If the size of the aluminum particles is bigger than the thickness of the fluidized bed, $d > l$, the diameter of the aggregate is represented by the following formula[1]:

$$D_{ag} = \sqrt[3]{\left[\frac{6lD_e^2}{\pi\beta} + 2h_{Al}^2 n_{Al}\left(\frac{3d}{2} - h_{Al}\right) - d^3\right]N_{ag} + d^3} \tag{9}$$

Here '$h_{Al} = d - l$', is the height of the aluminum exposed the fluid bed top, '$n_{Al} = (D_e/d)^2$' is the number of aluminum particles in the fluid bed. The number of aggregation is calculated as follows:

$$N_{ag} = \frac{t_{ig}}{t_{ac}} = \frac{t_{ig}\dot{r}\beta\phi}{d\left(1 - \beta\phi\frac{l}{d}\right)} \tag{10}$$

The exposed area of the aluminum particle used in the calculation for '$t_{ig}$' can be calculated by the following formula.

$$A_{ex} = 2\pi(d/2)\dot{r}t \tag{11}$$

Here, it is assumed that the aluminum particles are exposed due to retraction of the fluid bed after the propellant combustion. From the above Eq. 11, the ignition time can be calculated by the following formula.

$$\begin{aligned}&\int_0^{t_{ig}} hA_{ex}dt \\ &= \rho_{Al}V_{Al}(c\Delta T + L) = \rho_{Al}\frac{3}{4}\pi\left(\frac{d}{2}\right)^3(c\Delta T + L)\end{aligned} \tag{12}$$

$$\int_0^{t_{ig}} 2\pi h(d/2)\dot{r}t\,dt = \rho_{Al}\frac{3}{4}\pi\left(\frac{d}{2}\right)^3(c\Delta T + L) \tag{13}$$

$$t_{ig} = \sqrt{\frac{4}{3}\frac{\rho_{Al}R^2}{h\dot{r}}(c\Delta T + L)} \tag{14}$$

The propellant burning rate is given by[13]:

$$\dot{r} = 0.000891\, p^{0.84775}\,[cm/\mathrm{sec}] \tag{15}$$

In Eq. 9, the diameter of the agglomerates '$D_{ag}$' is the arithmetic mean of the volume or

mass. The size distribution of the Al(l)/$Al_2O_3$(l) droplets of the AP/HTPB/Al composites, after combustion, is assumed to be log-normal. In this work, the probability density function(PDF) is obtained by log-normal curve fitting[16]:

$$f(\overline{D_i}) = \frac{1.5}{\overline{D_i}\sigma\sqrt{2\pi}} \exp\left(-\frac{\left(\ln \overline{D_i}\right)^2}{2\sigma^2}\right) \quad (16)$$

Here, '$D_i$', is the representative diameter, '$D_m$' is the scale parameter, '$\sigma$' is the shape parameter and is assumed to be 1 in this case and $\overline{D_i} = \frac{D_i}{D_m}$.

The scale parameter '$D_m$' is iteratively adjusted to the value with which '$D_{43}$' of PDF satisfies '$D_{ag}$', where

$$D_{43} = \frac{\sum_{i=1}^{N} f(\overline{D_i}) D_i^4}{\sum_{i=1}^{N} f(\overline{D_i}) D_i^3} \quad (17)$$

### 2.2 Validation of the Agglomeration Model

To verify the accuracy of the model, the predicted results were compared with the experimental data by Sambamurthy et al.[17] for the micro-sized and by Babuk[18] for nano-sized initial Al-particles. Sambamurthy's data are for PBAN whereas the present model is for HTPB, however because HTPB and PBAN have very similar characteristics, PBAN experimental results can be used for the model verification. Refer the Table 1 the error for 30 $\mu m$ initial Al-particle was relatively low 2.6%. While, for nano-sized Al-particle/HTPB propellants, there is a lack of experimental data. Therefore, for model verification for the case of nano-sized Al-additive propellants, Babuk's work, which refers to HMX and inert binder, had to be used. The characteristic '$l$' and '$h$' values are also unavailable in Babuk's work and therefore these values are obtained from Sambamurthy's work. Due to these reasons, there is an error of 16% between the experimental and theoretical values and is within the acceptable limits.

Table 1. Experimental verification result.

| Init. Al-Dia. [$\mu m$] | Chamber Condition | Fuel | Perchlorate | $D_{ag}$[$\mu m$] Expt./Theo. |
|---|---|---|---|---|
| | | Mass fraction (%) | Size [$\mu m$] | Error (%) |
| 30 | 1.38 $MPa$ | AP/PBAN/Al | AP | 193/198 |
| | | 71/11/18 | 390 | 2.6 |
| 0.179 | 6 $MPa$, 1400 $K$ | AP/HMX/inert binder/Al | AP/HMX | 20/16.8 |
| | | 50/20/14/16 | 160-315 | 16 |

## 3. Mechanical Erosion Formulation

### 3.1 Discrete Phase Governing Equations

The trajectory of Al(l)/$Al_2O_3$(l) droplets are tracked through Lagrangian model. In this approach, after every certain number of continuous phase(Euler phase) iterations, the trajectories of parcels(group of particles, here a group of droplets)are calculated according to the set of droplet-gas interaction equations. In the real case, the number of droplets will be too large to practically track each of them individually in a simulation. To solve this problem, instead of droplets, parcels are tracked that will represent the behavior of all the droplets. These parcels can be thought of as a bundle of droplets. This whole approach falls under the Lagrangian multiphase model, also sometimes known as Discrete Phase Model(DPM). This model is valid only if the total volume of the droplets is less than 10%

of the gas phase volume and the droplet-droplet interaction is negligible.

The drag force on one single droplet is defined as:

$$F_d = \frac{1}{2} C_d \rho A_p |v_p| v_p \quad (18)$$

Where, '$C_d$', '$A_P$' and '$v_P$' are Schiller-Naumann[19] drag coefficient, projected area of the droplet and droplet slip velocity respectively. Pressure gradient force is given by:

$$F_p = - V_p \nabla p_{static} \quad (19)$$

'Vp' is the volume of the droplet. The heat transfer equation for a single droplet is given as:

$$m_p c_p \frac{dT_p}{dt} = Q_t + Q_{rad} \quad (20)$$

Ranz-Marshall[20] correlation was used to determine the heat transfer coefficient. All the momentum and energy sources for the droplets act as a sink for the continuous phase, thereby enabling coupling between the two phases. Aluminum particle combustion was not simulated.

### 3.2 Mechanical Erosion Model

There is no openly available experimental data on mechanical erosion by Al(l)/$Al_2O_3$(l) droplets in the solid rocket motor environment. The erosion rate is defined as the mass of wall material eroded per unit area per unit time. It is calculated on wall faces by accumulating the damage that each particle impact does on the face[21]. Mathematically, this is defined by the following equation:

$$E_f (Kg/s/m^2) = \frac{1}{A_f} \sum_{\pi(f)} m_\pi e_r \quad (21)$$

Where, '$E_f$' is erosion rate, '$A_f$' the face area, '$m_\pi$' is the mass flow rate of particles in parcel impacting on the face, '$e_r$' is the erosion ratio[21]. Theoretically, erosion ratio '$e_r$' is defined as the amount of wall material removed per mass of the particle impinging on the wall surface. The summation is over all parcels which strike the face in a Lagrangian iteration. The erosion rate therefore depends on the flow (whether and how particles impact on the wall) and the chosen method for the erosion ratio[21].

Empirical model given by Oka et al.[22] and Oka and Yoshida[23], calibrated[24] for the rocket nozzle environment, is incorporated in the present simulation to predict the mechanical erosion. The model is shown below Eq. 22 and the model constants are presented in Table 2[24].

$$e_r = g(a) e_{ref} \left(\frac{U}{U_{ref}}\right)^{k_2} \left(\frac{D}{D_{ref}}\right)^{k_3} \quad (22)$$

Where,

$$g(a) = (\sin\alpha)^{n_1} [1 + H_v (1 - \sin\alpha)]^{n_2} \quad (23)$$

In the Eq. 22 and Eq. 23, '$U$' is the velocity magnitude of the droplets impinging on the wall, '$\alpha$' is angle of attack with respect to the wall face normal, '$U_{ref}$', '$D_{ref}$' and '$e_r$' are the reference particle velocity, particle diameter and erosion ratio, respectively. Their values are based on Neilson and Gilchrist experimental work[25] on erosion by a stream of solid particles. '$H_v$' is the Vickers hardness for graphite in GPa. Exponent $n_1$ and $n_2$ in Oka et al.[22] model depends on material

Table 2. Oka's model parameters.

| Parameters | Value |
|---|---|
| $U_{ref}$ | 110.6 $m/s$ |
| $D_{ref}$ | 297 $\mu m$ |
| $e_{ref}$ | 0.065 |
| $H_v$ | 0.228 $GPa$ |
| $n_1$ | 0.793 |
| $n_2$ | 0.762 |
| $k_2$ | 2.0 |
| $k_3$ | 0.0 |

properties and particle shape. For '$k_2$' and '$k_3$', their theoretical values are taken from Ref.[22]. In SRM, Al(l)/$Al_2O_3$(l) is present as liquid droplets. Therefore, the use of solid particle data in the mechanical erosion correlations will lead to errors. As the solid particle will cause more erosion than the liquid droplets, the predicted erosion by this co-relation will represent the worst case scenario[24].

### 3.3 Assumptions and Boundary Conditions

The Al(l)/$Al_2O_3$(l) droplets are modeled as spherical droplets, whereas in reality, Al(l) and $Al_2O_3$(l) are immiscible liquids, and $Al_2O_3$(l) is present as a cap on the Al(l) droplet. AP/HTPB/Al is taken as the reference fuel, with mass fraction of 71/14/15. For an assumed propellant burning rate of 9.0678 mm/s and density of 1.794 $g/cm^3$[26], the mass generation rate will be 16.273 $kg/m^2/s$. Chamber pressure and temperature are 6.8MPa and 3327 $K$ respectively. In Thakre et al.[24] simulation, 10% of Al was assumed to remain unburnt at the propellant surface and forms $Al_2O_3$ smoke after combustion. The rest of Al gets oxidized to form Al(l)/$Al_2O_3$(l)-droplets. Here it is assumed that the unburnt 10% Al undergoes complete combustion within very short distance from burning surface and the species mass fractions given in Ref.[24] are accordingly modified as in Table 3 to get the new species mass fraction after the 10% Al gets completely oxidized. The nozzle wall is assumed to be at a constant temperature of 2500 $K$. In reality, the wall temperature at the solid-gas interface may vary from 2200 $K$ to 2800 $K$ along the wall. The input condition for the Lagrangian phase are also presented in Table 4.

Table 3. Gaseous propellant(Eulerian) mass inflow conditions.

| Species | Mass fraction |
|---|---|
| $H_2O$ | 0.109111 |
| CO | 0.284957 |
| $CO_2$ | 0.022013 |
| $H_2$ | 0.022267 |
| $Al_2O_3$ | 0.232293 |
| HCl | 0.230154 |
| $N_2$ | 0.099204 |
| Inlet flow conditions | |
| $P_0$ | 6.8 $MPa$ |
| $T_0$ | 3327 $K$ |

Table 4. Dispersed phase(Lagrangian) mass inlet conditions.

| Species | Multi component Al(l)/$Al_2O_3$(l) |
|---|---|
| **Mass flux** ($kg/m^2/s$) | 0.122<br>0.830 |
| **Injection temperature** ($K$) | 2350 |
| **Droplet diameter for differentd cases** ($\mu m$) | 103.9<br>97.5<br>90.0<br>70.1<br>45.9<br>15.7 |
| **Injection velocity** ($m/s$) | 0.1<br>(vertically downwards) |

## 4. Results and Discussion

### 4.1 Agglomeration Model

From presented agglomeration mode, the

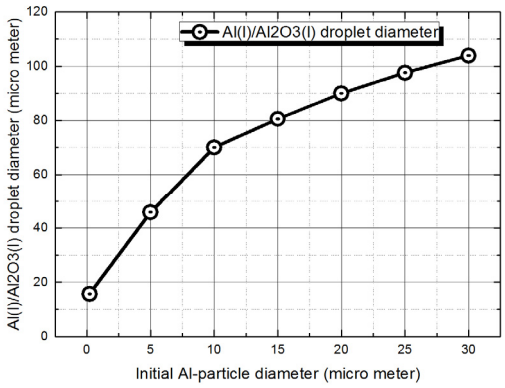


Fig. 1 Arithmetic Mean $Al(l)/Al_2O_3(l)$-droplet diameter variation with Initial Al-particle diameter.

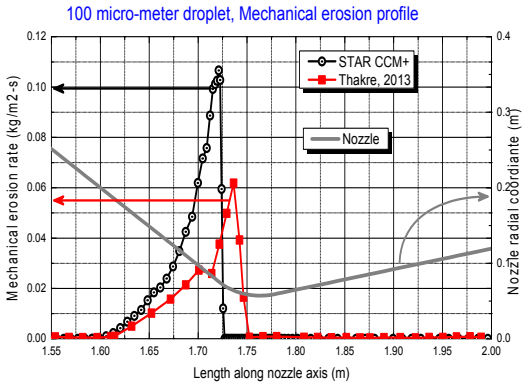


Fig. 2 100 micro meter mechanical erosion comparison with Thakre et al.[1].

$Al(l)/Al_2O_3(l)$-droplet diameter plot(Fig. 1) we can see that the $Al(l)/Al_2O_3(l)$-droplet size increases with the increase in initial diameter of Al(l)-particles present in the solid fuel. Smaller Al-particles produce smaller Al-agglomerates. Reduction in the Al-agglomerate size, ensures their complete combustion and enhances Isp. Mechanical erosion rate also falls down as the $Al(l)/Al_2O_3(l)$-droplet size decreases. These favorable characteristics of nano-sized Al-particles make them more favorable ingredients of solid fuels.

### 4.2 CFD Modelling

A well refined grid is made, with $y^+ < 1$. To account for the turbulent dispersion, 6 parcels were injected at each injection location. Overall the total number of parcel streams were 1200(=200×6). Fig. 2 shows the mechanical erosion comparison with Thakre et al.[24] results. The present work results seem to over predict the ablation. The large difference in the result is attributed to the non-availability of exact geometry in the open literature and the difference in droplet size distribution. In the present work the geometry was generated by digitizing the image file of Fig. 3 from Ref.[12]. Also, Thakre et al. used log-normal droplet size distribution with mean droplet size of 100 $\mu m$ and log10 standard deviation of 0.2, whereas the present comparison case uses uniform droplet diameter of 100 $\mu m$. Nonetheless, the present mechanical erosion model predicts the location of maximum erosion rate very accurately.

### 4.3 Effect of particle size on the gas flow field

From Fig. 3 it can be seen that the smaller 15.7 $\mu m$ droplets followed the gas path more closely as compared to the larger 103.9 $\mu m$ droplets. Both larger and smaller droplets enter the gas phase at a velocity of 0.1 $m/s$, larger droplets have higher momentum and their trajectory is less influenced by the gas flow as compared to that of the smaller droplets. In the highlighted parts as shown in Fig. 3, the heavier droplets travelled a longer vertical distance(left box) whereas the lighter droplets gained the axial momentum in a shorter distance. Before the throat region, both heavier and lighter droplets had a velocity component in the radially inward direction, in the diverging section the gas flow expands

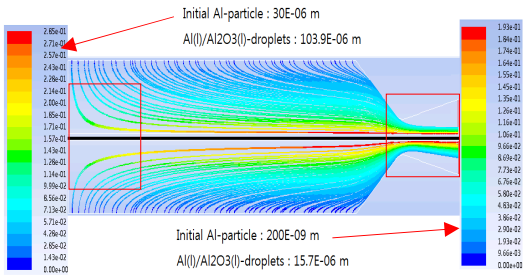


Fig. 3 droplet residence time contours.

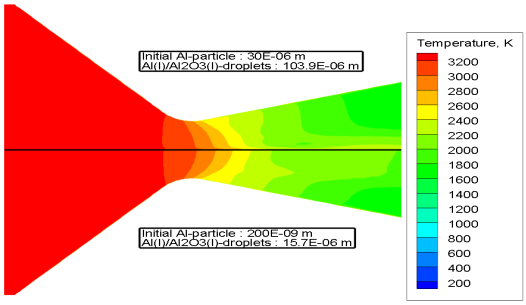


Fig. 5 Temperature contours(K).

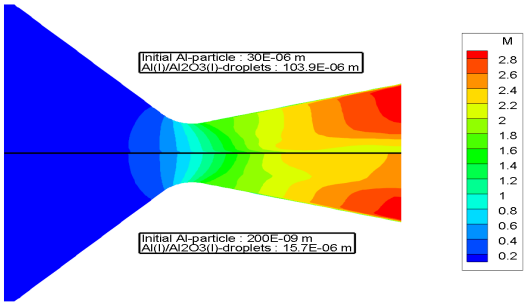


Fig. 4 Mach number contours(M).

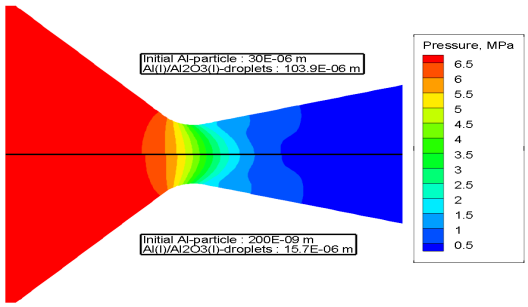


Fig. 6 Pressure contours(MPa).

and provides the radially outward momentum to the droplets. These two opposing effects almost nullify for the case of 103.9 $\mu m$ droplets and they exit the throat and nozzle with negligible radial velocity. On the other hand, the lighter 15.7 $\mu m$ droplets gain radially outward momentum in the divergent section of the nozzle. It takes longer to accelerate the bigger(heavier) droplets and thus the bigger droplets took longer to escape from the nozzle, as compared to lighter (smaller) droplets.

In Fig. 4 the Mach contours for the case of 103.9 $\mu m$ droplet are more perturbed in comparison to that of the 15.7 $\mu m$ droplet case, this is because larger droplets travelled almost axially in the divergent part whereas the lighter droplets followed the gas flow and spread more uniformly in the divergent section and the effect of particles on the gas glow field is diffused out in a larger region. With similar arguments the disturbances in the temperature field Fig. 5 can also be explained. The pressure wave propagates at acoustic speed and thus there is negligible effect on the pressure field, as can be seen in Fig. 6. It can be said, that as the droplet size decreases, the characteristic discrete phase properties becomes less prominent and the droplets behave more like a continuous phase.

### 4.4 Particle size effect on the mechanical erosion rate

Mechanical erosion for different droplet sizes is shown in Fig. 7, as expected the erosion rate is significant in the convergent section only, in the divergent section, no erosion is recorded because droplets traveled almost axially and did not interact at all with the nozzle wall. The maximum erosion rate takes place slightly ahead of the throat and then

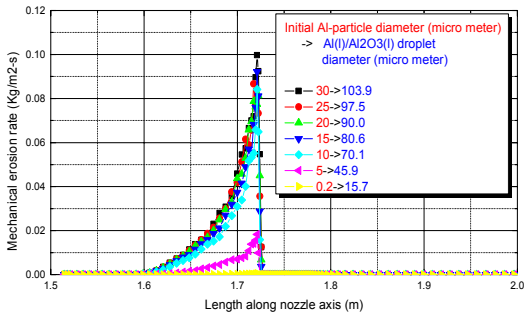


Fig. 7 Mechanical erosion rate variation with mean Al(l)/$Al_2O_3$(l)-droplet diameter(the graphs of this Fig. are off-set horizontally and are shown in Fig. 8 for clarity).

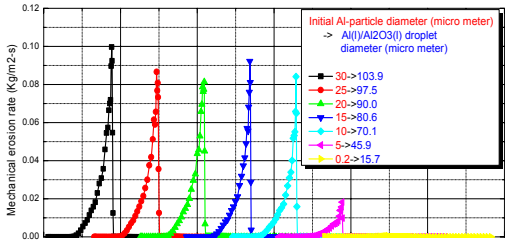


Fig. 8 Comparison of mechanical erosion rate fordifferent mean Al(l)/$Al_2O_3$(l)-droplet diameter(graphs are off-set horizontally).

suddenly falls down to zero. Mechanical erosion variation graphs can be seen more clearly in Fig. 8 Comparison of mechanical erosion rate for different mean Al(l)/$Al_2O_3$(l)-droplet diameter(graphs are off-set horizontally) Fig. 8, the axial coordinates for the nozzles are off-set. It can be seen that the erosion rate remains almost unchanged until the Al(l)/$Al_2O_3$(l)-droplet diameter drops to 45.9 $\mu m$. This can be explained using the erosion ratio model of Eq. 22, it is a function of angle of attack '$\alpha$' and impact speed '$U$'. Eq. 22 suggests that erosion ratio will be higher for higher angle of attack and higher velocity and vice versa. As the Al(l)/$Al_2O_3$(l)-droplet diameter decrease, they follow the gas flow more closely, consequently their trajectory becomes more tangential to the wall (decrease in '$\alpha$') and their velocity increases. Below a certain diameter, almost all the droplets travels nearly tangential to the wall in the convergent section and the effect of increase in velocity of droplets becomes redundant. Consequently, the erosion rate falls almost to zero for very small diameters like 15.7 $\mu m$.

Experimental data[27] for various carbon-carbon based rocket motors suggests mechanical erosion rates in the range of 0.0 ~ 0.169 $kg/m^2s$. The erosion rate predicted in the present study falls in this range.

## 5. Conclusion

Theoretical model for the calculation of Al-agglomerates was established. The results of the model were found to match very closely with the experimental data. Based on the Al-agglomerate size, the mean Al(l)/$Al_2O_3$(l) diameter was also calculated. The calculated erosion rate and erosion profile were observed to be similar to the existing ones[24,27]. Thus it can be concluded that the presented model for agglomerate size calculation and solution setup for mechanical erosion rate are reasonably satisfactory to study the trend of mechanical erosion variation with the agglomerate size. And from the results we can conclude that using smaller size of additive Al particle such as nano-size, the Al(l)/$Al_2O_3$(l) droplet size decreases and the discrete phase starts following the gas flow more and more closely. As the droplet size is reduced, the mechanical erosion rate also decreased, because the interaction between dispersed phase and wall reduced with the reduction in droplet size. From the above arguments, it can be

concluded that it is advantageous to use nano-sized Al additives to decrase the mechanical erosion rate.

## Acknowledgment

The authors would like to acknowledge the financial support from the Research Fund of Agency for Defense Development regarding "A study on Heat Flux and Ablation Prediction Technique of Rocket Nozzle by Nano Scale Two Phase Flow Using Statistical Mechanics" (ADD-13-01-05-15)

## References

1. Yavor, Y., Gany, A. and Beckstead, M.W., "Modeling of the Agglomeration Phenomenon in Combustion of Aluminized Composite Solid Propellant," *Propellants, Explosives, Pyrotechnics*, Vol. 39, Issue 1, pp. 108-116, 2014.
2. Kuo, K.K. and Acharya, R., *Application of Turbulent and Multiphase Combustion*, John Wiley & Sons, Inc., New York, NY, USA, 2012.
3. Crump, J.E., Prentice, J.L. and Kraeutle, K.J., "Role of Scanning Electron Microscope in Study of Solid Propellant Combustion: Behavior of Metal Additives," *Combustion Science and Technology*, Vol. 1, Issue 3, pp. 205-223, 1969.
4. Gany, A., Caveny, L.H. and Summerfield, M., "Aluminized Solid Propellant Burning in a Rocket Motor Flow Field," *AIAA Journal*, Vol. 16, No. 7, pp. 736-739, 1978.
5. Price, E.W., "Combustion of Metallized Propellants, in: Fundamentals of Solid Propellant Combustion, Progress in Astronautics and Aeronautics," *AIAA Journal*, Vol. 90, pp. 479-513, 1984.
6. Boraas, S., "Modeling Slag Deposition in the Space Shuttle Solid Rocket Motor," *Journal of Spacecraft and Rockets*, Vol. 21, No. 1, pp. 47-54, 1984.
7. Salita, M., "Deficiencies and Requirements in Modeling of Slag Generation in Solid Rocket Motors," *Journal of Propulsion and Power*, Vol. 11, No. 1, pp. 10-23, 1995.
8. Beckstead, M.W., "An Overview of Aluminum Agglomeration Modeling," *50th Israel Annual Conference on Aerospace Sciences*, Haifa, Israel, pp. 834-861, 25-26, Feb. 2010.
9. Cohen, N.S., "A Pocket Model for Aluminum Agglomeration in Composite Propellants," *AIAA Journal*, Vol. 21, No. 5, pp. 720-725, 1983.
10. Crump, J.E., "Aluminum Combustion in Composite Propellants," *Interagency Chemical Rocket Propulsion Group: Combustion Instability Conference*, Silver Spring, MD, USA, CPIA Publ. No. 105, May 1966.
11. Gallier, S., "A Stochastic Pocket Model for Aluminum Agglomeration in Solid Propellants," *Propellants, Explosives, Pyrotechnics*, Vol. 34, Issue 2, pp. 97-105, 2009.
12. Thakre, P., Rawat, R., Clayton, R. and Yang, V., "Mechanical Erosion of Graphite Nozzle Material in Solid-Propellant Rocket Motors," *448th AIAA Aerospace Sciences Meeting Including the New Horizons Forum and Aerospace Exposition*, Orlando, FL, USA, AIAA 2010-615, Aug. 2010.
13. Tanner, M.W., "Multidimensional Modeling of Solid Propellant Burning Rates and Aluminum Agglomeration and One-Dimensional Modeling of RDX/GAP and AP/HTPB," Ph.D. Dissertation,

Department of Chemical Engineering, Brigham Young University, Provo, USA, 2008.

14. Yetter, R.A., Risha, G.A. and Son, S.F., "Metal Particle Combustion and Nanotechnology," *Proceeding of the combustion institute*, Vol. 32, No. 2, pp. 1819-1938, 2009.
15. Gany, A. and Caveny, L.H., "Agglomeration and Ignition Mechanism of Aluminum Particles in Solid Propellants," *17th Symposium (International) on combustion*, Vols. 20-25, pp. 1453-1461, Aug. 1978.
16. Jackson, T.L., Najjar, F. and Buckmaster, J., "New Aluminum Agglomeration Models and Their Use in Solid-Propellant-Rocket Simulations," *Journal of propulsion and power*, Vol. 21, No. 5, pp. 925-936, 2005.
17. Sambamurthi, J.K., Price, E.W. and Robert, K.S., "Aluminum Agglomeration in Soli-Propellant Combustion," *AIAA Journal*, Vol. 22, No. 8, pp. 1132-1138, 1984.
18. Babuk, V., Dolotkazin, I., Gamsov, A., Glebov, A., DeLuca, L.T. and Galfetti, L., "Nanoaluminum as a Solid Propellant Fuel," *Journal of Propulsion and Power*, Vol. 25, No. 2, pp. 482-489, 2009.
19. Schiller, L. and Naumann, A., "Ueber die grundlegenden Berechnungen bei der Schwerkraftaufbereitung," *VDI Zeits*, Vol. 77, No. 12, pp. 318-320, 1933.
20. Ranz, W.E. and Marshall, W.R., "Evaporation from Drops--Part I and II p. 141," *Chemical Engineering Progress*, Vol. 48, No. 3, pp. 141, 1952.
21. CD-Adapco, "User Guide STAR-CCM+," Vol. Version 10.04, Seoul, Korea, 2015.
22. Oka, Y.I., Okamura, K. and Yoshida, T., "Practical Estimation of Erosion Damage caused by Solid Particle Impact. Part 1: Effect of Impact Parameters on a Predictive Equation," *Wear*, Vol. 259, Issues 1-6, pp. 95-101, 2005.
23. Oka, Y.I. and Yoshida, T., "Practical Estimation of Erosion Damage caused by Solid Particle Impact. Part 2: Mechanical Properties of Materials directly Associated with Erosion Damage," *Wear*, Vol. 259, Issues 1-6, pp. 102-109, 2005.
24. Thakre, P., Rawat, R., Clayton, R. and Yang, V., "Mechanical Erosion of Graphite Nozzle in Solid-Propellant Rocket Motor," *Journal of Propulsion and Power*, Vol. 29, No. 3, pp. 593-601, 2013.
25. Ranz, W.E. and Marshall, W.R., "Evaporation from Drops--Part I and II p. 141," *Chemical Engineering Progress*, Vol. 48, No. 3, pp. 141, 1952.
26. Sabnis, J., "Numerical Simulation of Distributed Combustion in Solid-Rocket Motor with Metallized Propellant," *Journal of Propulsion and Power*, Vol. 19, No. 1, pp. 48-55, 2003.
27. Ketner, D.M. and Hess, H.S., "Particle Impingement Erosion," *15th Joint Propulsion Conference*, Las Vegas, NV, USA, AIAA Paper 79-1250, June 1979.